Bone 120 (2019) 50–60

Contents lists available at ScienceDirect

Bone

journal homepage: www.elsevier.com/locate/bone

Full Length Article

Lowering iron level protects against bone loss in focally irradiated and contralateral femurs through distinct mechanisms

Jian Zhang[a,b,1], Lijun Zheng[a,b,1], Ziyang Wang[a,b], Hailong Pei[a,b], Wentao Hu[a,b], Jing Nie[a,b], Peng Shang[c,d], Bingyan Li[a,e], Tom K. Hei[a,b,f,*], Guangming Zhou[a,b,**]

[a] State Key Laboratory of Radiation Medicine and Protection, School of Radiation Medicine and Protection, Medical College of Soochow University, Suzhou, China
[b] Collaborative Innovation Center of Radiation Medicine of Jiangsu Higher Education Institutions, Suzhou, China
[c] Key Laboratory for Space Bioscience and Biotechnology, Institute of Special Environmental Biophysics, School of Life Sciences, Northwestern Polytechnical University, Xi'an, China
[d] Research & Development Institute in Shenzhen, Northwestern Polytechnical University, Shenzhen, China
[e] Department of Nutrition and Food Hygiene, School of Public Health, Medical College of Soochow University, Suzhou, China
[f] Center for Radiological Research, College of Physician and Surgeons, Columbia University, New York, USA

ARTICLE INFO

Keywords:
Ionizing radiation
Bone loss
Iron homeostasis
Osteoclasts
Hepcidin

ABSTRACT

Radiation therapy leads to increased risk of late-onset fragility and bone fracture due to the loss of bone mass. On the other hand, iron overloading causes osteoporosis by enhancing bone resorption. It has been shown that total body irradiation increases iron level, but whether the systemic bone loss is related to the changes in iron level and hepcidin regulation following bone irradiation remains unknown. To investigate the potential link between them, we first created an animal model of radiation-induced systemic bone loss by targeting the mid-shaft femur with a single 2 Gy dose of X-rays. We found that mid-shaft femur focal irradiation led to structural deterioration in the distal region of the trabecular bone with increased osteoclasts surface and expressions of bone resorption markers in both irradiated and contralateral femurs relative to non-irradiated controls. Following irradiation, reduced hepcidin activity of the liver contributed to elevated iron levels in the serum and liver. By injecting hepcidin or deferoxamine (an iron chelator) to reduce iron level, deterioration of trabecular bone microarchitecture in irradiated mice was abrogated. The ability of iron chelation to inhibit radiation-induced osteoclast differentiation was observed in vitro as well. We further showed that ionizing radiation (IR) directly stimulated osteoclast differentiation and bone resorption in bone marrow cells isolated not from contralateral femurs but from directly irradiated femurs. These results suggest that increased iron levels after focal radiation is at least one of the main reasons for systemic bone loss. Furthermore, bone loss in directly irradiated bones is not only due to the elevated iron level, but also from increased osteoclast differentiation. In contrast, the bone loss in the contralateral femurs is mainly due to the elevated iron level induced by IR alone. These novel findings provide proof-of-principle evidence for the use of iron chelation or hepcidin as therapeutic treatments for IR-induced osteoporosis.

Abbreviations: BMD, bone mineral density; BV/TV, bone volume fraction; BS, bone surface; BFR/BS, bone formation rate/bone surface; CFU-F, CFU-fibroblast; CFU-Ob, CFU-osteoblast; Car2, carbonic anhydrase II; CTSK, cathepsin K; DFO, deferoxamine mesylate; FPN1, ferroportin 1; FBS, fetal bovine serum; GAPDH, glyceraldehyde 3-phosphate dehydrogenase; HE, hematoxylin and eosin; Hepc, hepcidin-1; IR, ionizing radiation; μCT, micro-computed tomography; MAR, mineral apposition rate; MS/BS, mineralizing surface/bone surface; MMP9, matrix metallopeptidase 9; M-CSF, macrophage colony-stimulating factor; MSCs, mesenchymal stem cells; NFATc1, nuclear factor of activated T-cells, cytoplasmic 1; NF-κB, nuclear factor-kappa B; Ob.Pm/B.Pm, osteoblast perimeter/bone perimeter; Oc.Pm/B.Pm, osteoclast perimeter/bone perimeter; OCPs, Osteoclast progenitors; PBS, phosphate buffer saline; RANKL, receptor activator for nuclear factor-κ B ligand; SD, standard deviation; Tb.Th, trabecular thickness; Th.Sp, trabecular separation; Tb.N, trabecular number; TRAP, tartrate-resistant acid phosphatase; TfR1, transferrin receptor 1; Veh, vehicle

* Correspondence to: T.K. Hei, 630 West 168th Street, VC11-205, New York, NY 10032, United States of America.
** Correspondence to: G. Zhou, 199 Renai Road, Suzhou 215123, China.
E-mail addresses: tkh1@cumc.columbia.edu (T.K. Hei), gmzhou@suda.edu.cn (G. Zhou).
[1] These authors equally contributed to this work.

https://doi.org/10.1016/j.bone.2018.10.005
Received 4 July 2018; Received in revised form 21 September 2018; Accepted 6 October 2018
Available online 07 October 2018

1. Introduction

Radiation therapy is a highly targeted and effective modality in the clinical management of malignancies. Although significant improvements have been made with precise treatment planning and delivery, the area selected for irradiation usually includes the whole tumor plus the immediate surrounding normal tissue resulting in delayed side effects. Irradiation of the bone frequently leads to bone loss and increased risk of fractures [1], a condition commonly seen in patients with various cancers [2–5]. Furthermore, there is evidence of an abscopal effect in bone loss following single limb irradiation in that bone loss occurs not only at irradiated site, but at the contralateral, non-irradiated side as well [6–9]. The underlying mechanism is not well understood yet. Uncovering the mechanisms of both direct and indirect effects of radiation on bone are of great importance for developing preventive and curative treatment strategies.

Iron metabolism is closely related to bone homeostasis. Increased iron level contributes to bone loss, characterized by enhanced bone resorption and decreased bone formation. Osteoporosis frequently occurs in patients with hemochromatosis, African hemosiderosis, thalassemia or sickle cell disease that are associated with systemic iron overload [10]. There is evidence that an increase in total body iron storage is associated with high rate of bone loss in healthy postmenopausal women and middle-aged men [11]. These data suggest that enhanced iron storage could be an independent risk factor for accelerated bone loss, even in healthy populations [11]. Hepcidin, secreted by liver, is a key hormone that regulates iron homeostasis in the body. Hepcidin acts to lower iron in the blood by binding to and degrading the export protein ferroportin 1 (FPN1) [12]. Deficiency in hepcidin causes iron overload, which in turn upregulates hepcidin expression in a feedback mechanism [13]. Recent studies demonstrate that total body irradiation immediately increases serum iron in mice in a dose-dependent manner, which could persist for three weeks or even longer [14,15]. It is not clear whether increased iron storage occurs in the body after focal bone irradiation and whether the process is mediated by altered hepcidin expression. Furthermore, the question whether increased serum iron contributes to the systemic bone loss following radiation remains unanswered.

Since single limb irradiation could induce systemic bone loss and radiation has been shown to increase iron storage, we posed the hypothesis that increased iron storage induced by focal ionizing radiation (IR) mediated the subsequent systemic bone loss. Earlier reports on systemic bone loss utilized mostly large irradiated area covering the whole or large regions of hind-limb [7–9], a scenario that cannot recapitulate focal radiotherapy. In this study, we used a Small Animal Image Guided Irradiation System to precisely irradiate the mid-shaft of left femur in male C57BL/6 mice with a single dose of 2 Gy. The radiation was delivered in a circle collimated field with a diameter of 5 mm. Therefore, focally irradiated areas included only the bone marrow cavity and cortical bone of the mid-shaft and avoided the direct damage to both the distal and proximal trabecular bone. In the present study, we reported microarchitectural deterioration and activated osteoclast differentiation in irradiated and out of field, contralateral distal femurs. The systemic bone loss was associated with an abscopal effect on the liver resulting in elevated serum iron levels through down-regulation of hepcidin. Notably, IR directly stimulated local bone loss in irradiated bone. We further demonstrated in an animal model that lowering iron levels by injecting iron chelator, deferoxamine mesylate (DFO), and hepcidin 1 offered protection against IR-induced either systemic or local bone loss.

2. Material and methods

2.1. Animal study design

All animal studies described in this article were approved by the Animal Ethics and Welfare Committee at Soochow University. 4-week-old male C57BL/6J mice were purchased from and raised in laboratory animal center of Soochow University. The mice were fed with a standard pellet diet and distilled water ad libitum. Mice were group housed under standard vivarium with a 12 h light-dark cycle, at a temperature of 23 °C–25 °C and a relative humidity of 40 ± 5%. After acclimation, a Small Animal Image Guided Irradiation System (Precision X-Ray, North Branford, CT, USA) were used to precisely irradiate the mid-shaft of left femur at a single dose of 2 Gy on day 1. This system offers integrated precision irradiation with cone beam CT guidance and treatment planning systems with dose calculation tools based on Monte Carlo methods. Radiation was delivered in a circle collimated field with a diameter of 5 mm at a rate of 0.23 Gy/s. Control mice were similarly manipulated, and underwent cone beam CT scan. A single 2 Gy dose was used in the present study to simulate clinical radiotherapy setting consistent with previous studies on radiation-induced bone loss [7,16].

DFO (250 mg/kg; Sigma-Aldrich, St. Louis, MO, USA) and hepcidin-1 (500 μg/kg; Bachem AG, Bubendorf, Switzerland) or an equivalent volume of saline were injected intraperitoneally every other day. The subcutaneous injections started 2 days before irradiation and continued until the animals were sacrificed 28 days after radiation. The mice without DFO or hepcidin-1 treatment were sacrificed one week and four weeks after irradiation, respectively.

2.2. Micro-computed tomography (μCT) analysis

One and four weeks after radiation, femurs were harvested for μCT analyses (Skycan-1174, Bruker, Kontich, Belgium). Trabecular bone microarchitecture was evaluated in the distal metaphysis of the femur in a region that began 0.5 mm proximal to the growth plate and extended proximally 1 mm. Geometric trabecular analysis included bone mineral density (BMD), bone volume fraction (BV/TV), bone surface (BS), trabecular thickness (Tb.Th), trabecular separation (Th.Sp), and trabecular number (Tb.N). These parameters were calculated in accordance with guidelines for use of μCT in rodents [17].

2.3. Dynamic histomorphometry

Mice were injected subcutaneously with calcein (35 mg/kg; Sigma-Aldrich) 10 days and 3 days, respectively, before dissection. 28 days after irradiation, femurs were harvested, fixed in 75% ethanol, and then embedded with methyl methacrylate. Longitudinal sections were cut at 8 μm thickness for dynamic measurements. Pictures were taken using a fluorescence microscopy (Leica Microsystems GmbH, Wetzlar, Germany). Image J software (National Institutes of Health, Bethesda, MD; http://imagej.nih.gov/ij/) was used to measure and analyze the following dynamic parameters: mineral apposition rate (MAR; μm/day), mineralizing surface/bone surface (MS/BS; %), and bone formation rate/bone surface (BFR/BS; mm^3/mm^2/day).

2.4. Histology

Bilateral femurs were harvested 4 weeks after radiation for histological analysis. Briefly, the femurs were fixed in 4% paraformaldehyde for 2 days, decalcified in 10% EDTA for 21 days, and processed for paraffin sections. The sections were stained with hematoxylin and eosin (H&E), and with tartrate-resistant acid phosphatase (TRAP) stain. The osteoblast perimeter (Ob.Pm/B.Pm) and osteoclast perimeter (Oc.Pm/B.Pm) were quantified relative to the bone surface. The sections were viewed on a light microscope (Leica Microsystems GmbH) and analyzed by ImageJ software (National Institutes of Health).

2.5. CFU-F and CFU-Ob assays for bone marrow mesenchymal stem cells

Bilateral femurs were harvested one day after irradiation. Bone marrow cells of medullary cavities were collected individually from

irradiated and contralateral femurs. Cell number was determined using a hemocytometer after removal of red blood cells. For CFU-fibroblast (CFU-F) assays, 1×10^5 cells were seeded in 35 mm dish in α-Minimum Essential Medium (α-MEM; Gibco, Grand Island, NY, USA) supplemented with 10% fetal bovine serum (FBS; Gibco), and 2 mM L-glutamine (Amresco, Solon, OH, USA). On day 14, cultures were fixed by 70% ethyl alcohol and stained with 0.1% crystal violet. For CFU-osteoblast (CFU-Ob) assays, the cells were cultured with 10 mM β-glycerophosphate (Sigma-Aldrich) and 50 mg/mL ascorbic acid (Sigma-Aldrich) for 21 days, and stained with Alizarin Red (Sigma-Aldrich). The colony-forming efficiency was determined by the number of colonies formed in a 35 mm dish.

2.6. Osteoclastogenesis assays

The effects of irradiation on osteoclast differentiation were examined with bone marrow cells isolated from irradiated and contralateral femurs one day after irradiation. Bone marrow cells were individually flushed from bilateral femurs, and cultured in α-MEM supplemented with 10% FBS, and 2 mM L-glutamine. For osteoclastogenesis assays, bone marrow cells were seeded at a density of 2×10^4 cells/cm^2 and incubated with 50 ng/mL macrophage colony-stimulating factor (M-CSF; Pepro Tech, Rocky Hill, NJ, USA) and 50 ng/mL receptor activator for nuclear factor-κ B ligand (RANKL; Pepro Tech) for 6 days, with exchange fresh medium containing M-CSF and RANKL every other day. The mature osteoclasts were determined by TRAP staining using a Leukocyte Acid Phosphatase kit (Sigma-Aldrich). Multinucleated (> 3 nuclei) TRAP-positive cells were quantified by Image J software (National Institutes of Health). For bone resorption assay, bone marrow cells were seeded at a density of 2×10^4 cells/cm^2 on an Osteo Assay Plate (Corning, Tewksbury, MA, USA), and incubated with M-CSF (50 ng/mL) and RANKL (50 ng/mL) for 2 weeks. The plate was bleached by 0.5% sodium hypochlorite and resorbed pits were visualized using a light microscope (Leica Microsystems GmbH).

Osteoclast progenitors (OCPs) were used for DFO treatment experiments in vitro. Bone marrow cells were flushed from femurs, and cultured in α-MEM supplemented with 10% FBS, 2 mM L-glutamine, and 10 ng/mL M-CSF (PeproTech). The non-adherent cells were transferred to a new dish the next day and cultured with M-CSF for 3 days to obtain OCPs. OCPs induced from non-treated mice were seeded at a density of 1×10^4 cells/cm^2 and cultured overnight. Then the OCPs were treated with DFO (100 μM) for 6 h, and irradiated with 2 Gy using 225 kV X-rays at a dose rate of 0.23 Gy/s (Precision X-Ray). After that, the medium were supplemented with DFO (100 μM), M-CSF (50 ng/mL) and RANKL (50 ng/mL), and changed every other day for 6 days. Osteoclast formation and bone resorption potential were separately evaluated using TRAP staining and bone resorption pit assay as described above.

2.7. Measurement of iron parameters

Iron concentration was determined with a colorimetric assay kit (Nanjing Jian cheng, Nanjing, China) for iron quantification. Ferritin and hepcidin in serum were measured using a mouse serum ELISA kit (Shanghai Meilian, Shanghai, China). To investigate the iron distribution in liver, deparaffinized sections were stained with Perls Prussian blue kit (Solarbio, Beijing, China) and counterstained with eosin.

2.8. Western blot

Femurs and livers were harvested at various time points after radiation for western blot assay. They were frozen in liquid nitrogen and stored at −80 °C. The tissue proteins were extracted using a DNA/RNA/Protein isolation kit (Omega Bio-tek, Norcross, GA, USA) according to the manufacturer's protocol. Equal amounts of total protein were loaded onto 10% SDS-PAGE gel. The proteins were transferred onto a nitrocellulose membrane, blocked in phosphate buffer saline (PBS) containing 5% milk, and incubated with primary antibody against nuclear factor of activated T-cells, cytoplasmic 1 (NFATc1; Abcam, Cambridge, MA, UK), nuclear factor-kappa B (NF-κB; Cell Signaling Technology, Boston, MA, USA), transferrin receptor 1 (TfR1; Thermo Fisher, Rockford, IL, USA), ferritin (Abcam), FPN1 (Thermo Fisher), hepdidin-1 (Abcam), and glyceraldehyde 3-phosphate dehydrogenase (GAPDH; Cell Signaling Technology) overnight at 4 °C, followed by horseradish peroxides-linked secondary antibody (Beyotime) for 1 h at room temperature. GAPDH was used as an internal control.

2.9. Quantitative real-time PCR

Femurs were harvested four weeks after irradiation, frozen in liquid nitrogen and stored at −80 °C. Total RNA was extracted by a DNA/RNA/Protein isolation kit (Omega Bio-tek), reversely transcribed, and processed for PCR reactions according to the manufacturer's protocol (TaKaRa, Dalian, China). Quantitative real-time PCR was performed on the ViiA 7 Real-Time PCR System (Applied Biosystems, Foster, CA, USA). The amplification program was as follows: pre-denaturation at 95 °C for 10 min, followed by 40 cycles of 95 °C for 10 s, annealing temperature for 20 s and 72 °C for 20 s. The data were normalized to GAPDH and analyzed via the $2^{-\Delta\Delta Ct}$ method. The following primers were used: carbonic anhydrase II (Car2), 5′-CATTACTGTCAGCAGCGAGCA-3′ and 5′-GACGCCAGTTGTCCACCATC-3′; cathepsin K (CTSK), 5′-CAGCAGAACGGAGGCATTGA-3′ and 5′-CCTTTGCCGTGGCGTTATAC-3′; matrix metallopeptidase 9 (MMP9), 5′-GCCCTGGAACTCACACGACA-3′ and 5′-TTGGAAACTCACACGCCAGAA-3′; GAPDH, 5′-TGCACCACCAACTGCTTAG-3′ and 5′-GGATGCAGGGATGATGTTC-3′.

2.10. Statistical analysis

Data were expressed as means ± standard deviation (SD) and were analyzed by one-way ANOVA with Newman-Keuls, by paired Student's *t*-test for comparison of irradiated and non-irradiated contralateral femurs or by unpaired Student's *t*-test, as appropriate (GraphPad, La Jolla, CA, USA). Differences with $P < 0.05$ were considered statistically significant.

3. Results

3.1. Focal irradiation of the left femur caused deterioration of trabecular bone in bilateral femurs

Local and systemic effects of focal radiation to the left femoral shaft were determined by analysis of femur microarchitecture using μCT. The irradiated field size was a circle with a diameter of only 5 mm, avoiding direct damage to the distal femur. Irradiated femurs and contralateral femurs were compared with those from non-irradiated controls. According to previous research, bone loss occurs as early as one week post irradiation [7,18–20]. Therefore, we chose one week as an early time point. 7 days post-irradiation, CT imaging showed clear deteriorated trabecular microarchitecture in both irradiated and contralateral femurs with a reduction in bone mineral density (BMD, 19% and 19%, respectively, when compared with non-irradiated control), bone volume fraction (BV/TV, 17% and 18%, respectively), and trabecular thickness (Tb.Th, 16% and 17%, respectively) accompanied by increases in trabecular separation (Tb.Sp, 31% and 31%, respectively) (Fig. 1A–G). After 28 days, the trabecular microarchitecture showed further deterioration than what was observed on day 7 in both irradiated and contralateral femurs (Fig. 1A) with a marked decrease in BMD (15% and 14%, respectively relative to controls), BV/TV (42% and 36%, respectively), BS (38% and 35%, respectively), Tb.Th (17% and 13%, respectively), and trabecular number (Tb.N, 30% and 26%, respectively) accompanied by increases in Tb.Sp (62% and 50%, respectively) (Fig. 1A-G). Furthermore, compared with non-irradiated

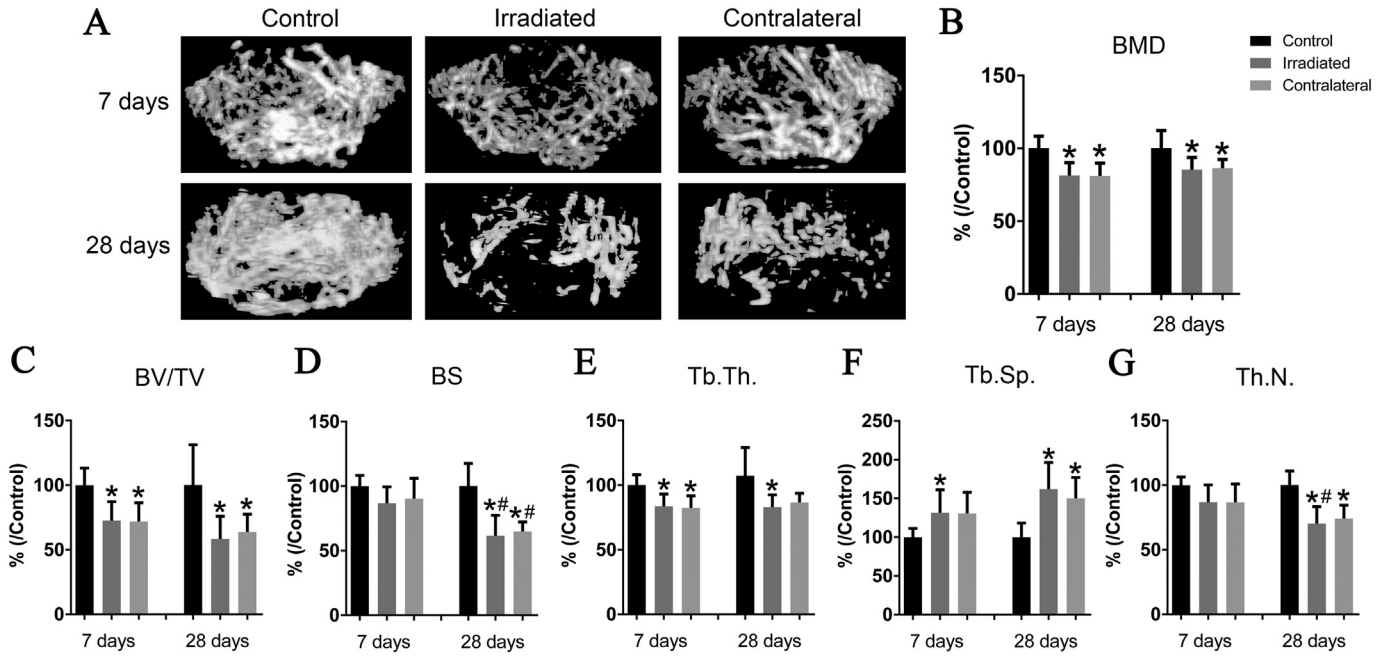

Fig. 1. Effects of IR exposure to the midshaft of left femur on trabecular microarchitecture in irradiated and contralateral femurs 7 days and 28 days postirradiatin relative to control mice, as assessed by μCT. (A) Representative three-dimensional images of trabecular bone in the distal femur. (B–G) μCT measurements for bone mineral density (BMD), bone volume fraction (BV/TV), bone surface (BS), trabecular thickness (Tb.Th.), trabecular separation (Th.Sp.), and trabecular number (Tb.N.). n = 7 femurs per group. Values were expressed as percentage changes relative to control. All data were presented as mean ± SD. *$P < 0.05$ Control vs. Irradiated or Contralateral. #$P < 0.05$ 28 days vs. 7 days.

control femurs, the BS in bilateral femurs, and Tb.N in irradiated femurs of irradiated mice on day 28 post-irradiation was significantly decreased relative to that on day 7 (Fig. 1D, G). Cortical bone microarchitecture at the femoral midshaft assessed by μCT did not alter between groups (data not shown). Taken together, the contralateral group exhibited deteriorated trabecular bone with time compared with the non-irradiated control group, suggesting there is a systemic effect of bone irradiation.

3.2. Focal irradiation of the left femur stimulated bone resorption in vivo

To understand how bone marrow irradiation induced bone damage, we performed bone histomorphometry on bilateral femurs from irradiated and control mice on day 28. Consistent with previous reports of increased osteoclasts following IR, exposure to 2 Gy X-rays induced a significantly increase in osteoclast surface (OC.Pm/B.Pm) of both irradiated and contralateral femurs compared with non-radiated mice after 28 days (Fig. 2A). To further evaluate the mechanism behind the osteoclast activity, we extracted proteins and RNAs of the whole femurs, and detected the expressions of genes associated with osteoclast differentiation. Compared with non-irradiated control, nuclear factor of activated T cells 1 (NFATc1) and nuclear factor-κB (NF-κB) were highly expressed in both irradiated and contralateral femurs (Fig. 2B). Genes engaged in bone resorption, including carbonic anhydrase II (Car2), cathepsin K (CTSK), and matrix metalloproteinase 9 (MMP9), were significantly upregulated in contralateral femurs (Fig. 2C).

To cross check previous reports of marrow adiposity after irradiation [7,21], we examined H&E stained bone section and, to our surprise, found little or no marrow adiposity in either the distal or midshaft of irradiated femurs (Fig. 2D). In addition, there was no difference in osteoblast surface (OB.Pm/B.Pm) as revealed by H&E sections (Fig. 2E). Osteoblast activity was determined by dynamic histomorphometric analyses. Although focal irradiation damaged trabecular microarchitecture, it did not affect mineral apposition rate (MAR; μm/day), mineralizing surface (MS/BS), and bone formation rate (BFR/BS; mm^3/mm^2/day) in either irradiated or contralateral femurs (Fig. 2F). There was also no altered MAR in cortical bone among groups. Taken together, these data suggest that bone resorption was stimulated in vivo, and that increased bone resorption rather than decreased bone formation is responsible for IR induced systemic bone loss.

3.3. Irradiation directly promoted osteoclast differentiation in vitro

The direct effects of IR on osteoclast differentiation were examined with bone marrow cells isolated from irradiated and contralateral femurs one day after irradiation. Osteoclast formation and bone resorption in bone marrow cells isolated from irradiated femur were markedly stimulated, whereas there was no difference between contralateral and control femurs (Fig. 3A, B). The effects of IR on bone marrow mesenchymal stem cells (MSCs) were examined using CFU-F and CFU-Ob assays with bone marrow cells isolated from irradiated and contralateral femurs. Colony number of CFU-F and CFU-Ob in bilateral femurs of irradiated mice did not alter compared with controls (Fig. 3C, D). The results show that osteoclast differentiation can be stimulated directly by radiation, which could be the main reason for bone loss in directly irradiated femur.

3.4. Iron storage level was increased following focal bone irradiation

In view of the close correlation between iron and bone homeostasis, we examined whether IR altered iron levels in the body. At 7 and 28 days post-radiation, serum iron concentration was significantly increased compared with non-irradiated mice (Fig. 4A). Serum ferritin, widely used in clinical practice as an indicator of iron storage status, was also increased (Fig. 4B). The liver is an important iron storage tissue of the organism. The iron content of the liver can reflect the iron storage level of the body to a certain extent. Compared with control mice, the iron content in the liver of irradiated mice was significantly higher ($P \leq 0.05$, Fig. 4C). Iron distribution indicated by Perls Prussian blue stain also showed that more irons was accumulated in the liver of irradiated mice (Fig. 4D). To further explore the underlying mechanism of iron accumulation in the liver, the expressions of several iron

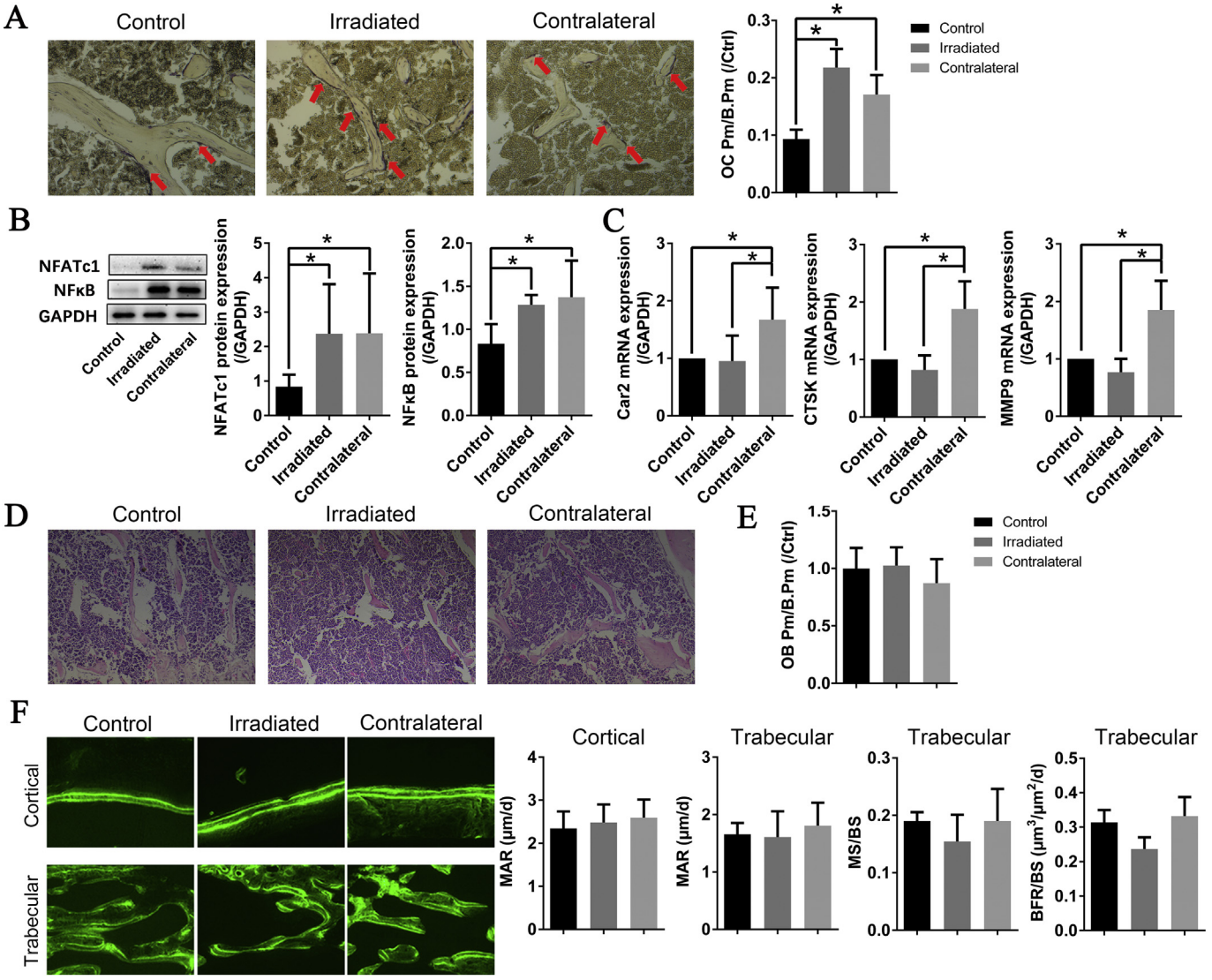

Fig. 2. Focal irradiation stimulates bone resorption and has no effects on bone formation. (A) Representative view of TRAP staining of distal femur trabecular bone from of irradiated and non-irradiated (contralateral) bone relative to control 28 days postirradiation. Arrowheads indicate TRAP positive osteoclasts. Osteoclast surface (OC.Pm/B.Pm) was quantified. n = 5 femurs/group. (B) Western blotanalysis of levels of NFATc1 and NFκB and (C) qPCR analysis of expressions of car2, CTSK and MMP9 from whole femur lysate of irradiated and non-irradiated (contralateral) bone relative to control 28 days postirradiation. n = 5 femurs/group. (D) Representative morphology of distal femur trabecula stained by HE staining at 28 days after irradiation. (E) Osteoblast surface (OB Pm/B·Pm) was quantified according to HE staining pictures. n = 5 femurs/group. (F) Representative calcein double labeling in the midshaft cortical bone and distal femur trabecula. Dynamic histomorphometric analysis quantifying mineral apposition rate (MAR; μm/day), mineralizing surface (MS/BS; %), and bone formation rate (BFR/BS; mm^3/mm^2/day). n = 5 femurs/group. All data were presented as mean ± SD. *$P < 0.05$ Control vs. Irradiated or Contralateral.

homeostasis proteins including TfR1 (involved in cellular iron import), ferritin (iron storage protein), and FPN1 (ferroportin, an iron export protein) were analyzed. Protein expression of TfR1 in the liver was not altered 7 days after focal irradiation, but increased by 28 days post-irradiation (Fig. 4E). Ferritin was upregulated on day 7 and 28. Moreover, FPN1 was reduced 28 days post-irradiation. Since focal irradiation increased iron storage level and caused bone loss in the contralateral femur, we next investigated whether focal irradiation had any effect on femur iron level. We found that TfR1 was elevated in both irradiated and contralateral femurs of irradiated mice compared with non-irradiated mice, indicating increased iron uptake (Fig. 4F). These results suggest the systemic upregulation of iron uptake in irradiated mice for both the liver and bilateral femurs. Increased iron level in the liver may be associated with increased expression of TfR1 and reduced FPN1.

3.5. Lowering iron level by DFO treatment blocked IR-induced trabecular deterioration

Since our results indicated that iron storage level and osteoclast activity were increased after focal irradiation, we hypothesized that an increase in the serum iron level is responsible for the systemic bone loss induced by IR. To test this hypothesis, mice were intraperitoneally injected with deferoxamine mesylate (DFO, an iron chelator), and changes in the distal trabecular bone of femurs in irradiated mice were examined. Treatment with DFO injections for 4 weeks, beginning 2 days before irradiation, blocked microarchitectural deterioration and increased BMD in both irradiated and contralateral area of femurs (Fig. 5A). In these animals, the trabecular microarchitectures were maintained to the same level as in non-irradiated group with control DFO treatment (Fig. 5B). In line with previous reports [22], we found that DFO treatment alone did not affect bone microarchitecture in non-irradiated, male mice when compared with vehicle-treated group

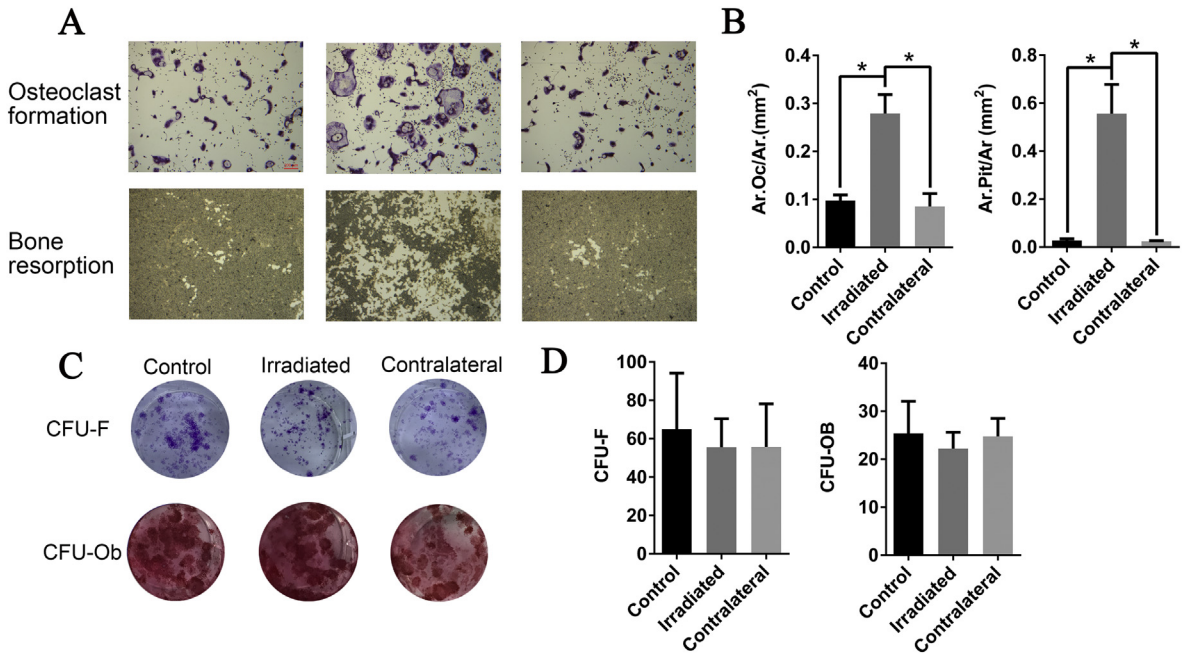

Fig. 3. Effects of IR on osteogenic and osteoclastogenic differentiation potential of bone marrow cells. Bone marrow cells were isolated from irradiated left femur and contralateral right femur of irradiated mice, and left femur of non-irradiated mice one day after focal irradiation. (A) Osteoclast formation was identified by TRAP positive cells with more than three nuclei after induced by MCSF and RANKL for 6 days. Bone resorption potential was identified by formed pits on after induced by MCSF and RANKL for 14 days. (B) Osteoclast formation was quantified by osteoclast area per square millimeter (Ar. Oc/Ar.). The potential of bone resorption was quantified by absorbed pits per square millimeter (Ar. Pit/Ar.). (C) CFU-F and CFU-Ob assay were performed with harvested bone marrow cells, and (D) quantified by number of colonies per 35 mm dish. n = 3 femurs per group. $^{*}P < 0.05$ Control vs. Irradiated or Contralateral.

(Fig. 5B). Furthermore, DFO treatment reversed the stimulative effects of IR on iron storage. After DFO was injected every other day for four weeks to irradiated animals, serum iron, serum ferritin, and ferritin protein levels were down-regulated to the control level (Fig. 5C–E). Since IR could directly promote osteoclast differentiation both in vivo and in vitro, we next investigated whether DFO treatment had inhibitory effects on osteoclast differentiation exposed to IR in vitro. Similar to our previous studies, radiation caused a remarkable increase in osteoclast formation and bone resorption. DFO completely inhibited osteoclast differentiation in both non-irradiated and irradiated cells (Fig. 5F, G). Taken together, our data indicate that lowering iron level by DFO treatment protected trabecular architecture of both irradiated and contralateral femurs, which could be mediated by reduced osteoclast activity.

3.6. Hepcidin treatment blocked IR induced trabecular deterioration

Hepcidin, secreted by hepatocytes, is a key regulator of systemic iron homeostasis, by negatively regulating the entry of iron into the circulation [23]. We investigated whether hepcidin was altered due to IR-induced high levels of iron. In vivo hepcidin levels were assessed in both the liver and serum of irradiated mice and were found to be downregulated (Fig. 6A, C). On the other hand, hepcidin injection partially but significantly reduced the serum iron concentration to the level as in control group (Fig. 6D). Furthermore, hepcidin-1 treatment did not affect its own expression in the liver of both non-irradiated (Control + Veh vs. Control + Hepc) and irradiated (Irradiated + Veh vs. Irradiated + Hepc) mice (Fig. 6B). Similarly, FPN1 expression in non-irradiated liver was also not affected by hepcidin-1 treatment (Control + Veh vs. Control + Hepc). Although focal irradiation down-regulated FPN1 expression, FPN1 expression was increased in Irradiated + Hepc group compared with Irradiated + Veh group at 4 weeks after irradiation (Fig. 6B). These results suggest that decreased hepcidin may be partially responsible for the elevated iron level in both the serum and liver of irradiated mice. To explore the potential of hepcidin-1 in alleviating radiation-induced bone loss, we investigated the protective effects of hepcidin-1 on trabecular bone in our mouse focal radiation model. 4 weeks of hepcidin injections, beginning 2 days before irradiation, not only blocked microarchitecture deterioration but also strikingly increased BMD and improved bone quality in bilateral femurs of the irradiated mice to the same levels as in control mice (Fig. 6E). Note that under the non-irradiated condition, hepcidin-1 did not influence trabecular microarchitecture (Control + Veh vs. Control + Hepc). These data indicate that elevating hepcidin-1 is effective in preventing radiation-induced bone loss by reducing iron levels.

4. Discussion

Among the various late effects of IR in the clinical management of cancer are bone complications, which include pathological fractures, inflammation and necrosis, growth delay and abnormal fracture healing [1–5]. In the present study, we demonstrated that focal irradiation of the bone resulted in an abscopal effect involving not only the bone but also the liver. Iron storage in both the serum and liver was significantly elevated after focal irradiation of the femur, and the lowering of iron level by the use of iron chelator or hepcidin reversed IR induced bone loss in irradiated and contralateral femurs. At relatively low dose of radiation exposure (usually < 2 Gy), the major cause for bone damage is the activation of bone resorption through osteoclast formation rather than suppression of bone formation [16]. The above findings are summarized in a model as shown in Fig. 7. These data provide the first evidence that systemic bone loss induced by focal femur irradiation is closely related with increased iron levels in the body, and that lowering of iron levels is capable of protecting the integrity of the trabecular bone after irradiation.

The bone remodeling balance between resorption by osteoclasts and formation by osteoblasts is pivotal for maintaining bone homeostasis [24]. IR can exert direct effects on both osteoclasts and osteoblasts in a dose dependent manner [16]. At relatively low doses (< 2 Gy), there is a marked decrease in trabecular bone mass as early as one week

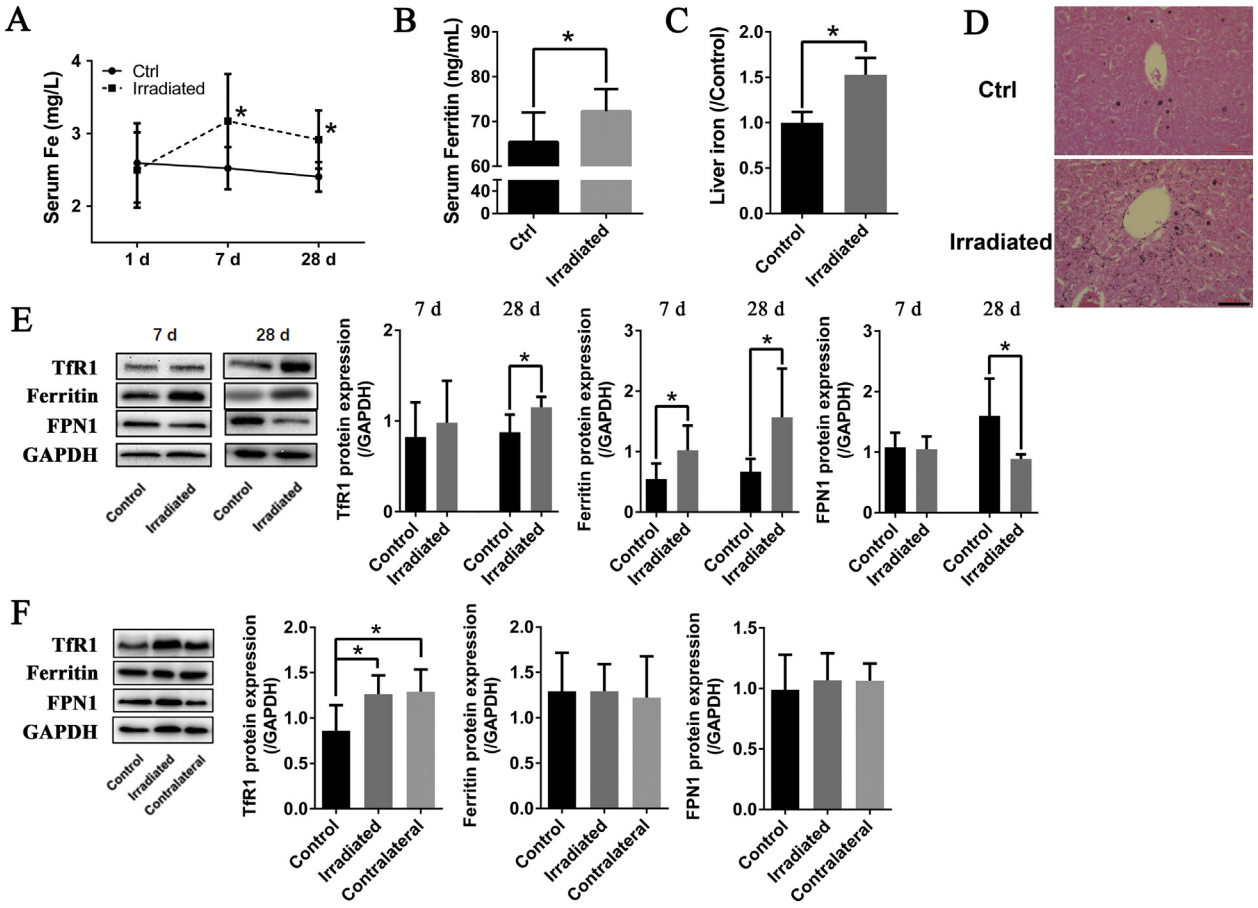

Fig. 4. Iron storage was increased in irradiated mice. (A) Serum iron concentration was increased at 7 days and 28 days after focal irradiation. n = 7 mice/group. (B) Serrum ferritin concentration was increased at 28 days after focal irradiation. n = 7 mice/group. (C) The content of iron in liver was increased 28 days after focal irradiation. n = 7 mice/group. (D) Iron distribution was visualized by Perls Prussian blue stain 28 days after irradiation. Compared with the non-irradiated group, there was more iron accumulation (blue dots) in the liver of irradiated mice. n = 7 mice/group. (E) Protein levels of TfR1, ferritin, and FPN1 in the liver of control and irradiated mice 7 and 28 days after irradiation. n = 6 mice/group. (F) Protein levels of TfR1, ferritin, and FPN1 in control, irradiated and contralateral femurs 28 days after irradiation. n = 6 mice/group. *$P < 0.05$ Control vs. Irradiated or Contralateral. (For interpretation of the references to colour in this figure legend, the reader is referred to the web version of this article.)

following exposure [7,19,25], due to elevated osteoclast activity [26,27]. Osteoclasts are large multinucleated cells derived from the myeloid lineage and are responsible for bone resorption [28]. As hematopoietic cells are extremely radiosensitive, there is evidence that osteoclast differentiation from their progenitors can be significantly induced at relatively low doses [7,26,27]. In the current study, we used a clinically relevant dose of 2 Gy for mid-shaft femur focal irradiation, and found elevated osteoclast activity in both irradiated and contralateral femurs compared with non-irradiated controls in vivo. Bone formation by osteoblasts was not affected after 2 Gy of irradiation both in vivo and in vitro. Our data provide support for the use of bisphosphonate in preventing bone loss in radiotherapy patients [16,29,30].

Though systemic bone loss and elevated osteoclast activity were observed in our irradiation model, the underlying mechanisms of osteoclast activation between irradiated femurs and contralateral femurs were not known. In this study, bone marrow cells isolated one day post-irradiation from the irradiated femur, but not from the contralateral one, had a significant increase in osteoclast formation and bone resorption. This suggests that the loss of trabecular bone in contralateral femur is not due to the direct stimulation of IR on osteoclast differentiation. On the other hand, we found elevated iron storage following focal irradiation, which was partially mediated by decreased expression of hepcidin in the liver. With bone marrow being the main site of iron utilization for hemoglobin synthesis by red blood cells (RBCs) and macrophages, primarily in the spleen, liver, and bone marrow, recycle iron by catabolizing senescent RBCs and export iron into bloodstream, excess iron is primarily stored in the liver [23]. After focal irradiation, we found that serum iron, serum ferritin, and liver iron were all elevated, suggesting an increase in iron storage in the body. Meanwhile, hepcidin expression was down-regulated in the liver. Hepcidin is a key regulator of the entry of iron into the circulation in mammals. Hepcidin inhibits iron transport by binding to the iron export channel FPN, which is located on the basolateral surface of gut enterocytes and cell surface of other cells. By inhibiting FPN, hepcidin prevents enterocytes from allowing iron into our body, and promotes iron release in other cells [23]. Therefore, if hepcidin was down-regulated, dietary iron absorption could be increased to some extent. The iron release from liver cells was also reduced by FPN inhibition, resulting in high iron store in the liver. From this point of view, dietary iron restriction is also beneficial for irradiated mice. Considering the tight correlation between iron overload and osteoclastogenesis, we used iron chelation treatment (e.g. DFO) to reduce the iron level in the body. In this way, DFO was found to protect against bone loss in both irradiated and contralateral femurs. DFO has been reported to inhibit osteoclastogenesis [22]. Our results further demonstrated that DFO treatment could completely inhibit osteoclast formation and bone resorption in vitro, whether the bone marrow cells were irradiated or not. In summary, iron chelation protects against IR induced bone loss through inhibiting osteoclast differentiation.

Cellular response to IR involves generation of endogenous reactive

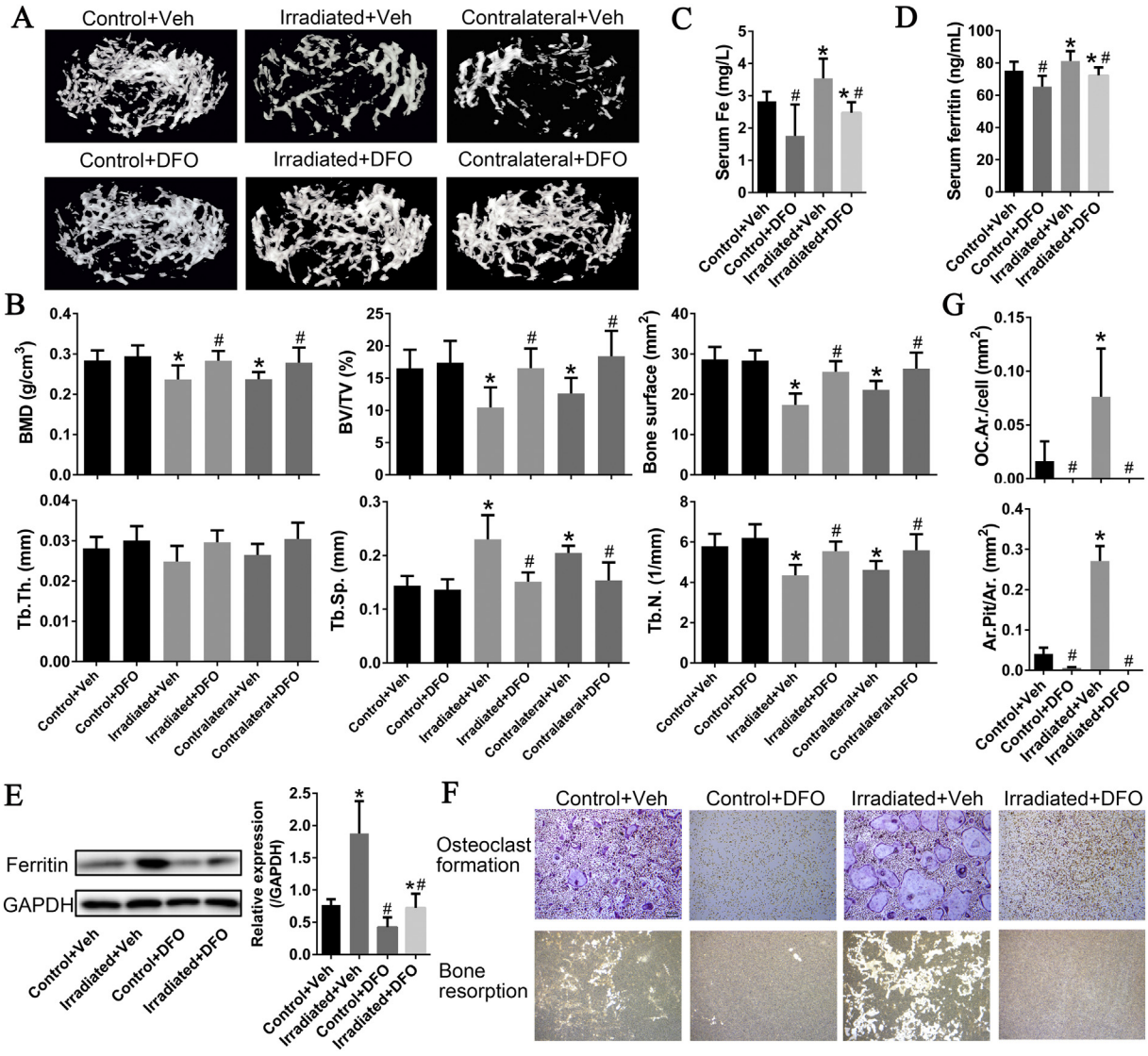

Fig. 5. DFO treatment reverses trabecular bone loss and microarchitectural deterioration caused by femur focal irradiation. (A) 3D reconstructed μCT images of trabecular bone of distal femurs in irradiated and control mice treated with and without DFO injections for 28 days after focal irradiation. n = 7 femurs/group. (B) μCT measurements for bone mineral density (BMD), bone volume fraction (BV/TV), bone surface (BS), trabecular thickness (Tb.Th.), trabecular separation (Th.Sp.), and trabecular number (Tb.N.). (C) Serum iron and (D) serum ferritin was determined in mice 28 days after irradiation with or without DFO treatment. n = 7 femurs/group. (E) Ferritin protein levels of mouse livers in mice 28 days after irradiation with or without DFO treatment. n = 6 femurs/group. (F) DFO inhibited radiation-stimulated osteoclast differentiation in vitro. OCPs were pretreated with DFO for 6 h and then received 2 Gy of X-Ray exposure. After that, osteoclast differentiation was induced by incubating with M-CSF and RANKL 6 days for osteoclast formation and 14 days for pits assay respectively. n = 3. Veh, vehicle; DFO, deferoxamine mesylate. #$P < 0.05$ Veh vs. DFO; *$P < 0.05$ Control vs. Irradiated or Contralateral.

oxygen species (ROS), leading to biological effects [31]. Upon exposure to relatively low-dose irradiation, IR can directly stimulate osteoclast differentiation [16]. Accumulating evidence indicates that such increase in endogenous ROS is associated with mitochondria change and water radiolysis [31]. In the current study, DFO not only completely inhibited osteoclast differentiation in non-irradiated cells but also in irradiated cells. As an iron chelator, DFO can negatively affect mitochondrial function through decreased activity of the iron-sulfur cluster containing complexes I, II and III, leading to reduced ATP level [32]. Osteoclasts is in a state of high-energy demand during its differentiation [22]. Although IR induces amount of endogenous ROS, decreased energy production in mitochondria by DFO treatment inhibits osteoclast differentiation ultimately.

Hepcidin serves as a major regulator of systemic iron homeostasis and its overexpression alleviates iron overloading and vice versa [13]. Our study demonstrated a reduced hepcidin level in the liver after focal irradiation along with a high level of iron storage in both the liver and serum. Similar to effects of the iron chelator DFO, hepcidin injection reduced the serum iron concentration and protected against IR induced bone loss in both contralateral and irradiated femurs. The radio-protective effects of hepcidin was not due to direct effects on bone cells as hepcidin had been reported to promote osteoclast differentiation in vitro [33], but on reducing iron levels [34]. Consistently, hepcidin injection reduced iron levels in our focal irradiated mouse model. On the other hand, cytokines including growth differentiation factor 15 (GDF15), and interferon β (IFNβ), known to down-regulate hepcidin expression, have been shown to be highly elevated in immune cells after radiation exposure [35–38]. It is possible that signals secreted by irradiated bone marrow cells inhibit hepcidin expression in distant unexposed liver. Taken together, focal irradiation not only has abscopal effects on bone, but also on liver. Further studies are required to identify the molecular mediators from bone tissue to regulate iron homeostasis.

Iron overload is known to induce osteoporosis with enhanced

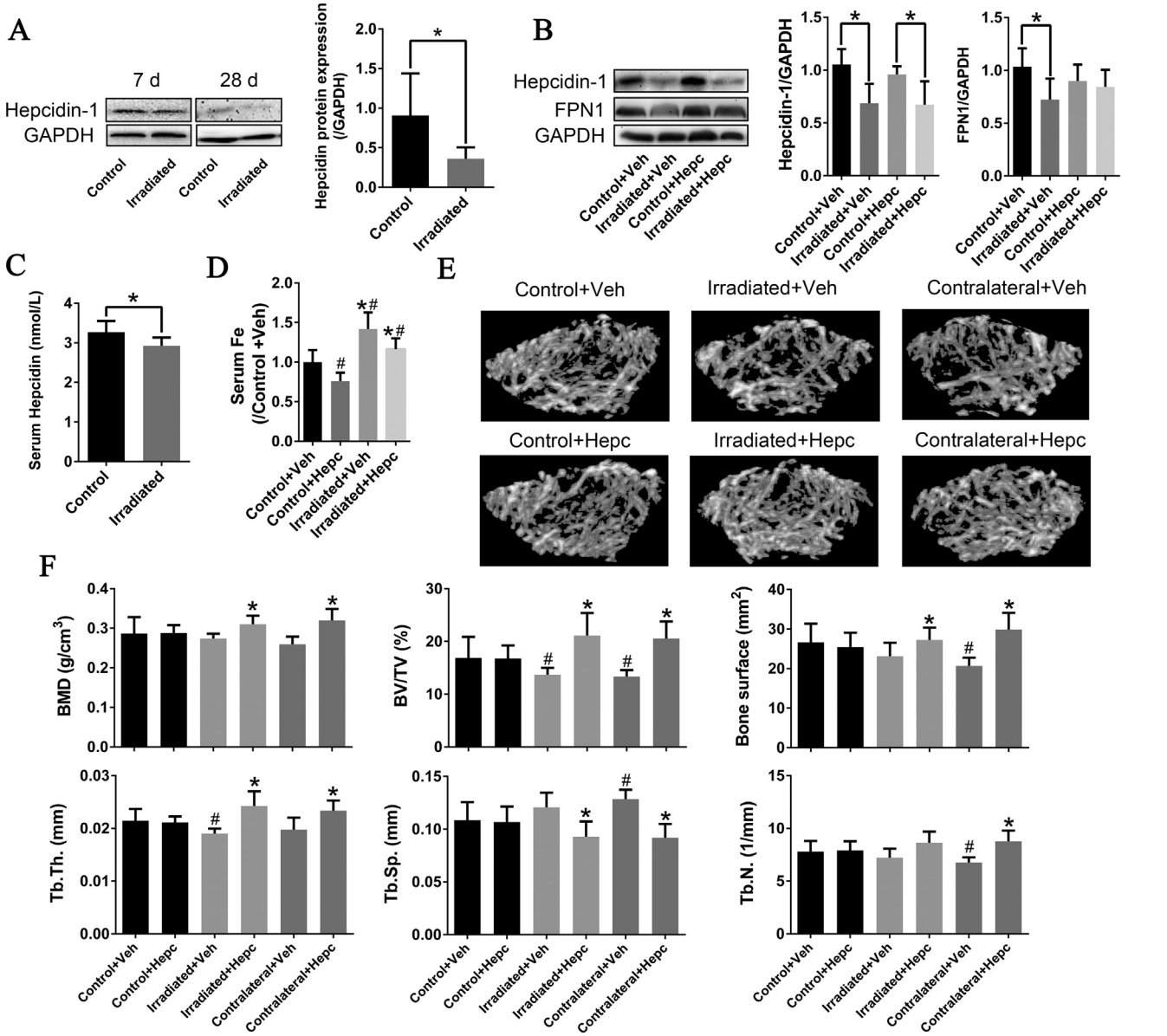

Fig. 6. Hepcidin treatment reverses trabecular bone loss and microarchitectural deterioration caused by femur focal irradiation. (A) Hepatic hepcidin-1 protein levels in irradiated and non-irradiated control mice at 7 days and 28 days after irradiation. n = 7 mice/group. (B) Hepatic protein levels of hepcidin-1 and FPN1 in mice 28 days after irradiation with or without hepcidin-1 treatment. n = 5 mice/group. (C) ELISA analysis of serum hepcidin concentrations of irradiated and non-irradiated control mice. n = 7 mice/group. (D) Serum iron was determined in mice 28 days after irradiation with or without DFO treatment. n = 7 mice/group. (E) Representative three-dimensional images of trabecular bone in the distal femur in irradiated and control mice treated with and without hepcidin-1 injections for 28 days after focal irradiation. n = 7 femurs/group. (F) μCT measurements for bone mineral density (BMD), bone volume fraction (BV/TV), bone surface (BS), trabecular thickness (Tb.Th.), trabecular separation (Th.Sp.), and trabecular number (Tb.N.). Veh, vehicle; DFO, deferoxamine mesylate; Hepc, hepcidin-1. #$P < 0.05$ Veh vs. DFO; *$P < 0.05$ Control vs. Irradiated or Contralateral.

osteoclastogenesis [10]. Our results showed that lowering iron levels in the serum by iron chelator or hepcidin could reverse the systemic bone loss induced by focal irradiation. This was likely a result of suppressed osteoclast activity. During osteoclast differentiation, iron uptake is enhanced via upregulated TfR1 [22]. Iron chelation (e.g. DFO) has been shown to improve bone quality by reducing osteoclast differentiation in iron-overload, ovariectomy and hind-limb unloading osteoporosis models [22,39,40]. In our study, TfR1 was highly expressed in both irradiated and contralateral femurs compared with control non-irradiated mice, suggesting increased iron uptake. We also found that iron chelation inhibited the direct stimulatory effects of IR on osteoclast differentiation. These data suggest that iron uptake by osteoclasts may be enhanced after IR, and iron is necessary for stimulatory effects of IR on osteoclast differentiation. Therefore, the bone loss in the irradiated bone is not only due to the elevated iron level following IR, but also from direct stimulatory effects of IR on osteoclast differentiation. Taken together, an increased iron level after focal radiation is at least one of the reasons for systemic bone loss outside the irradiation field.

There is evidence that iron chelator (e.g. DFO) has protective effects on IR induced bone damage in a rat model of distraction osteogenesis and in fracture healing after radiotherapy [41–43]. In addition to its inhibitory effects on osteoclastogenesis, DFO can augment vascularity and promote osteoblast differentiation via nuclear factor erythroid 2-related factor (Nrf2) mediated antioxidant pathway [44] and Wnt5a [45], which may be involved the improved bone union in pathologic fracture healing after radiotherapy. Our results show that DFO can abrogate IR induced osteoclast differentiation. In addition, our novel findings of the radio-protective effects of DFO and hepcidin on systemic

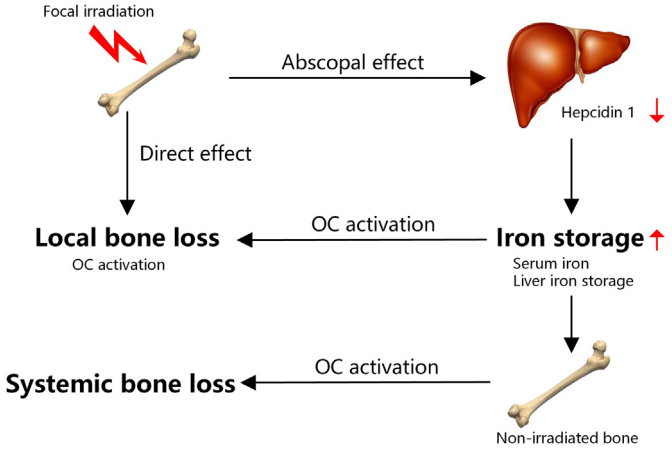

Fig. 7. Schematic representation of the underlying mechanisms for systemic bone loss induced by focal bone irradiation. Focal irradiation has an abscopal effect on the liver, reducing hepcidin expression that ultimately results in elevated iron availability in the body. The systemic bone loss outside the radiation field is mainly due to the increased osteoclast activation by elevated iron levels. The bone loss in the directly irradiated bone is not only due to the elevation of serum iron levels following induced by IR, but also from direct radiation-stimulated osteoclast differentiation. OC, osteoclast. Upward arrow: up-regulated. Downward arrow: down-regulated.

bone loss suggest the potential clinical efficacy of lowering iron storage during radiotherapy. Most important of all, iron reduction seems not to contribute to carcinogenesis in cancer patients receiving radiotherapy because there is a close link between increased body iron storage and increased cancer risk for excess iron [46].

5. Conclusions

In summary, our study reveals the first evidence that systemic bone loss induced by IR is related to the enhanced bone resorption due to elevated iron level in the body. Decreased hepcidin expression is responsible for this elevation of iron level. Lowering iron storage by iron chelator or hepcidin alleviates the radiation-induced deteriorated microarchitecture in trabecular bone. The bone loss in the irradiated field is not only due to the elevated iron level, but also from the direct stimulatory effects of IR on osteoclast differentiation. Overall, these results provide new perspectives for the underlying mechanisms of systemic bone loss. The therapeutic lowering of iron levels may be effective in the prevention and treatment of bone loss of patients undertaking radiotherapy.

Authors' contributions

JZ, TKH, and GZ designed the study. JZ, LZ, ZW, and JN conducted the experiments and analyzed the dada with HP, WH, PS, and BL. JZ, TKH, and GZ wrote the manuscript.

Conflicts of interest

There are no potential conflicts of interest related to this work.

Funding

This work was supported by the National Natural Science Foundation of China (31600674), Project funded by China Postdoctoral Science Foundation (2017M610352), and the Project Funded by the Priority Academic Program Development of Jiangsu Higher Education Institutions.

References

[1] M.J. Mitchell, P.M. Logan, Radiation-induced changes in bone, Radiographics 18 (1998) 1125–1136.
[2] N.N. Baxter, E.B. Habermann, J.E. Tepper, S.B. Durham, B.A. Virnig, Risk of pelvic fractures in older women following pelvic irradiation, JAMA 294 (20) (2005) 2587–2593.
[3] J.W. Kwon, S.J. Huh, Y.C. Yoon, S.H. Choi, J.Y. Jung, D. Oh, et al., Pelvic bone complications after radiation therapy of uterine cervical cancer: evaluation with MRI, AJR Am. J. Roentgenol. 191 (4) (2008) 987–994.
[4] S. Igdem, G. Alco, T. Ercan, M. Barlan, K. Ganiyusufoğlu, B. Unalan, et al., Insufficiency fractures after pelvic radiotherapy in patients with prostate cancer, Int. J. Radiat. Oncol. Biol. Phys. 77 (3) (2010) 818–823.
[5] H. Ikushima, K. Osaki, S. Furutani, K. Yamashita, Y. Kishida, T. Kudoh, et al., Pelvic bone complications following radiation therapy of gynecologic malignancies: clinical evaluation of radiation-induced pelvic insufficiency fractures, Gynecol. Oncol. 103 (3) (2006) 1100–1104.
[6] D. Jia, D. Gaddy, L.J. Suva, P.M. Corry, Rapid loss of bone mass and strength in mice after abdominal irradiation, Radiat. Res. 176 (5) (2011) 624–635.
[7] L.E. Wright, J.T. Buijs, H.S. Kim, L.E. Coats, A.M. Scheidler, S.K. John, et al., Single-limb irradiation induces local and systemic bone loss in a murine model, J. Bone Miner. Res. 30 (7) (2015) 1268–1279.
[8] M.E. Oest, C.G. Policastro, K.A. Mann, N.D. Zimmerman, T.A. Damron, Longitudinal effects of single hindlimb radiation therapy on bone strength and morphology at local and contralateral sites, J. Bone Miner. Res. 33 (1) (2018) 99–112.
[9] X. Xu, R. Li, Y. Zhou, Q. Zou, Q. Ding, J. Wang, et al., Dysregulated systemic lymphocytes affect the balance of osteogenic/adipogenic differentiation of bone mesenchymal stem cells after local irradiation, Stem Cell Res Ther 8 (1) (2017) 71.
[10] G.F. Li, Y.Z. Pan, P. Sirois, K. Li, Y.J. Xu, Iron homeostasis in osteoporosis and its clinical implications, Osteoporos. Int. 23 (10) (2012) 2403–2408.
[11] B.J. Kim, S.H. Ahn, S.J. Bae, E.H. Kim, S.H. Lee, H.K. Kim, et al., Iron overload accelerates bone loss in healthy postmenopausal women and middle-aged men: a 3-year retrospective longitudinal study, J. Bone Miner. Res. 27 (11) (2012) 2279–2290.
[12] E. Nemeth, M.S. Tuttle, J. Powelson, M.B. Vaughn, A. Donovan, D.M. Ward, et al., Hepcidin regulates cellular iron efflux by binding to ferroportin and inducing its internalization, Science 306 (5704) (2004) 2090–2093.
[13] T. Ganz, E. Nemeth, Hepcidin and disorders of iron metabolism, Annu. Rev. Med. 62 (2011) 347–360.
[14] X.H. Zhang, Z.C. Lou, A.L. Wang, X.D. Hu, H.Q. Zhang, Development of serum iron as a biological dosimeter in mice, Radiat. Res. 179 (6) (2013) 684–689.
[15] L.H. Xie, X.H. Zhang, X.D. Hu, X.Y. Min, Q.F. Zhou, H.Q. Zhang, Mechanisms of an increased level of serum iron in gamma-irradiated mice, Radiat. Environ. Biophys. 55 (1) (2016) 81–88.
[16] J. Zhang, X. Qiu, K. Xi, W. Hu, H. Pei, J. Nie, et al., Therapeutic ionizing radiation induced bone loss: a review of in vivo and in vitro findings, Connect. Tissue Res. (2018), https://doi.org/10.1080/03008207.2018.1439482.
[17] M.L. Bouxsein, S.K. Boyd, B.A. Christiansen, R.E. Guldberg, K.J. Jepsen, R. Müller, Guidelines for assessment of bone microstructure in rodents using micro-computed tomography, J. Bone Miner. Res. 25 (7) (2010) 1468–1486.
[18] A. Chandra, S. Lan, J. Zhu, T. Lin, X. Zhang, V.A. Siclari, et al., PTH prevents the adverse effects of focal radiation on bone architecture in young rats, Bone 55 (2) (2013) 449–457.
[19] H. Kondo, N.D. Searby, R. Mojarrab, J. Phillips, J. Alwood, K. Yumoto, et al., Total-body irradiation of postpubertal mice with (137)Cs acutely compromises the microarchitecture of cancellous bone and increases osteoclasts, Radiat. Res. 171 (3) (2009) 283–289.
[20] J.S. Alwood, M. Shahnazari, B. Chicana, A.S. Schreurs, A. Kumar, A. Bartolini, et al., Ionizing radiation stimulates expression of pro-osteoclastogenic genes in marrow and skeletal tissue, J. Interf. Cytokine Res. 35 (6) (2015) 480–487.
[21] X. Cao, X. Wu, D. Frassica, B. Yu, L. Pang, L. Xian, et al., Irradiation induces bone injury by damaging bone marrow microenvironment for stem cells, Proc. Natl. Acad. Sci. U. S. A. 108 (4) (2011) 1609–1614.
[22] K.A. Ishii, T. Fumoto, K. Iwai, S. Takeshita, M. Ito, N. Shimohata, et al., Coordination of PGC-1beta and iron uptake in mitochondrial biogenesis and osteoclast activation, Nat. Med. 15 (3) (2009) 259–266.
[23] D. Meynard, J.L. Babitt, H.Y. Lin, The liver: conductor of systemic iron balance, Blood 123 (2) (2014) 168–176.
[24] X. Feng, J.M. McDonald, Disorders of bone remodeling, Annu. Rev. Pathol. 6 (2011) 121–145.
[25] E.R. Bandstra, M.J. Pecaut, E.R. Anderson, J.S. Willey, F. De Carlo, S.R. Stock, et al., Long-term dose response of trabecular bone in mice to proton radiation, Radiat. Res. 169 (6) (2008) 607–614.
[26] J. Zhang, Z. Wang, A. Wu, J. Nie, H. Pei, W. Hu, et al., Differences in responses to X-ray exposure between osteoclast and osteoblast cells, J. Radiat. Res. 58 (6) (2017) 791–802.
[27] J.S. Willey, S.A. Lloyd, M.E. Robbins, J.D. Bourland, H. Smith-Sielicki, L.C. Bowman, et al., Early increase in osteoclast number in mice after whole-body irradiation with 2 Gy X rays, Radiat. Res. 170 (3) (2008) 388–392.
[28] W.J. Boyle, W.S. Simonet, D.L. Lacey, Osteoclast differentiation and activation, Nature 423 (6937) (2003) 337–342.
[29] J.S. Willey, E.W. Livingston, M.E. Robbins, J.D. Bourland, L. Tirado-Lee, H. Smith-Sielicki, et al., Risedronate prevents early radiation-induced osteoporosis in mice at multiple skeletal locations, Bone 46 (1) (2010) 101–111.
[30] L. Keenawinna, M.E. Oest, K.A. Mann, J. Spadaro, T.A. Damron, et al., Zoledronic

acid prevents loss of trabecular bone after focal irradiation in mice, Radiat. Res. 180 (1) (2013) 89–99.
[31] K. Kawamura, F. Qi, J. Kobayashi, Potential relationship between the biological effects of low-dose irradiation and mitochondrial ROS production, J. Radiat. Res. 59 (suppl_2) (2018) ii91–ii97.
[32] M.F. Hoes, N. Grote Beverborg, J.D. Kijlstra, J. Kuipers, D.W. Swinkels, B.N.G. Giepmans, et al., Iron deficiency impairs contractility of human cardiomyocytes through decreased mitochondrial function, Eur. J. Heart Fail. 20 (5) (2018) 910–919.
[33] G.Y. Zhao, D.H. Di, B. Wang, X. Huang, Y.J. Xu, Effects of mouse hepcidin 1 treatment on osteoclast differentiation and intracellular iron concentration, Inflammation 38 (2) (2015) 718–727.
[34] P. Zhang, S. Wang, L. Wang, B.C. Shan, H. Zhang, F. Yang, et al., Hepcidin is an endogenous protective factor for osteoporosis by reducing iron levels, J. Mol. Endocrinol. 60 (4) (2018) 297–306.
[35] P. Lee, H. Peng, T. Gelbart, L. Wang, E. Beutler, Regulation of hepcidin transcription by interleukin-1 and interleukin-6, Proc. Natl. Acad. Sci. U. S. A. 102 (6) (2005) 1906–1910.
[36] L. Deng, H. Liang, M. Xu, X. Yang, B. Burnette, A. Arina, et al., STING-dependent cytosolic DNA sensing promotes radiation-induced type I interferon-dependent antitumor immunity in immunogenic tumors, Immunity 41 (5) (2014) 843–852.
[37] N. Sandor, B. Schilling-Toth, E. Kis, A. Benedek, K. Lumniczky, G. Sáfrány, et al., Growth differentiation factor-15 (GDF-15) is a potential marker of radiation response and radiation sensitivity, Mutat. Res. Genet. Toxicol. Environ. Mutagen. 793 (2015) 142–149.
[38] T. Tanno, N.V. Bhanu, P.A. Oneal, S.H. Goh, P. Staker, Y.T. Lee, et al., High levels of GDF15 in thalassemia suppress expression of the iron regulatory protein hepcidin, Nat. Med. 13 (9) (2007) 1096–1101.
[39] B. Chen, Y.L. Yan, C. Liu, L. Bo, G.F. Li, H. Wang, et al., Therapeutic effect of deferoxamine on iron overload-induced inhibition of osteogenesis in a zebrafish model, Calcif. Tissue Int. 94 (3) (2014) 353–360.
[40] Z. Xu, W. Sun, Y. Li, S. Ling, C. Zhao, G. Zhong, et al., The regulation of iron metabolism by hepcidin contributes to unloading-induced bone loss, Bone 94 (2017) 152–161.
[41] A. Donneys, D.M. Weiss, S.S. Deshpande, S. Ahsan, C.N. Tchanque-Fossuo, D. Sarhaddi, et al., Localized deferoxamine injection augments vascularity and improves bony union in pathologic fracture healing after radiotherapy, Bone 52 (1) (2013) 318–325.
[42] P.A. Felice, S. Ahsan, A. Donneys, S.S. Deshpande, N.S. Nelson, S.R. Buchman, Deferoxamine administration delivers translational optimization of distraction osteogenesis in the irradiated mandible, Plast. Reconstr. Surg. 132 (4) (2013) 542–548.
[43] A. Donneys, S. Ahsan, J.E. Perosky, S.S. Deshpande, C.N. Tchanque-Fossuo, B. Levi, et al., Deferoxamine restores callus size, mineralization, and mechanical strength in fracture healing after radiotherapy, Plast. Reconstr. Surg. 131 (5) (2013) 711–719.
[44] J.H. Chung, Y.S. Kim, K. Noh, Y.M. Lee, S.W. Chang, E.C. Kim, Deferoxamine promotes osteoblastic differentiation in human periodontal ligament cells via the nuclear factor erythroid 2-related factor-mediated antioxidant signaling pathway, J. Periodontal Res. 49 (5) (2014) 563–573.
[45] U. Baschant, M. Rauner, E. Balaian, H. Weidner, A. Roetto, U. Platzbecker, et al., Wnt5a is a key target for the pro-osteogenic effects of iron chelation on osteoblast progenitors, Haematologica 101 (12) (2016) 1499–1507.
[46] S.V. Torti, F.M. Torti, Iron and cancer: more ore to be mined, Nat. Rev. Cancer 13 (5) (2013) 342–355.